THE JOURNAL OF PHYSICAL CHEMISTRY C

Article

Cite This: J. Phys. Chem. C 2019, 123, 29954−29963

pubs.acs.org/JPCC

Ligand-Mediated Nanocluster Formation with Classical and Autocatalytic Growth

Mohsen Farshad, Dylan Suvlu, and Jayendran C. Rasaiah*

Department of Chemistry, University of Maine, Orono, Maine 04469, United States

Supporting Information

ABSTRACT: We present a systematic study of ligand-mediated nanocluster (NC) formation using a kinetic model, which provides atomic insight into sub-nanometer cluster (S-NC) and NC formation. Our model describes the role of ligand-mediated nucleation and growth in obtaining monodisperse NCs. Nucleation includes metal ion reduction, reversible ligand association to the metal ion/atom, and formation of dimer nuclei. Growth can occur through autocatalytic surface growth and ligand-associated monomer addition to the cluster, depending on the rate of metal ion to neutral metal atom conversion. Furthermore, we studied the effect of the initial concentration of metal ions on NC formation using fast and slow reducing agents in the presence of slowly and rapidly binding ligands. The model shows that fast nucleation, slow growth, and a high molar ratio of rapidly binding ligand to metal ions promote the formation of S-NCs and NCs. Our results can guide experiments in the synthesis of ultrasmall clusters.

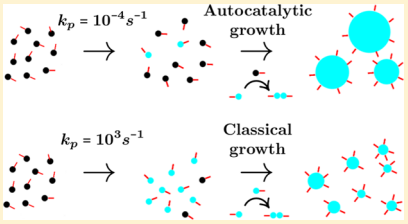

Nanoclusters (NCs) are clusters of metal atoms with diameters smaller than 2 nm and contain unique properties because of their small sizes.[1] Understanding their formation is useful for a variety of applications in catalysis,[2−6] bio-imaging and sensing,[7−10] and medical therapies.[11] The synthesis of atomically precise NCs is possible with meticulous control over experimental conditions, which requires knowledge of the variables that effect their sizes.[12] Advanced experimental techniques, such as liquid cell transmission electron microscopy, have allowed researchers to observe nanoparticle growth with unprecedented resolution.[13] Theoretical models have also unveiled many factors that affect the size of nanoparticles.[14,15] However, many key factors remain to be investigated. For example, what is the role of ligands in NC nucleation? Are they merely spectators, or do they play an important role in the nucleation process? Experiments provide insight into this process. For example, experiments on silver[16,17] and gold[18] nanoparticles without a strongly binding ligand show rapid growth of nanoparticles, in one case approaching diameters greater than 20 nm in a matter of milliseconds.[16] Experiments with strongly binding ligands (thiols or phosphine ligands), however, show stable NC synthesis with diameters less than 2 nm.[19,20] Here, we take steps toward finding the optimal conditions for sub-nanometer cluster (S-NC) formation and provide mechanistic insight into their ligand-mediated nucleation and growth. To pursue our intention, we developed a ligand-mediated kinetic model to investigate the formation of metal NCs starting from individual atoms (monomers) to the final stages of formation.

For several years, nanoparticle nucleation and growth were explained by LaMer's burst nucleation mechanism followed by nanoparticle growth.[21,22] LaMer's burst nucleation is based on Becker and Doring's classical nucleation theory.[21,22] In LaMer's nucleation mechanism, the concentration of monomers reaches a critical supersaturation point after which they nucleate by overcoming the energy barrier for nucleation.[23] This is followed by growth of nanoparticles as a separate step. However, experiments show that CNT fails to adequately describe nucleation and growth of transition-metal nanoparticles.[24,25] Finke and Watzky (FW) considered nucleation and growth occurring simultaneously through a two-step mechanism. In the FW model, slow, continuous nucleation occurs simultaneously with autocatalytic growth, which is controlled by the reaction rates.[24−26] Mozaffari et al. developed a model of ligand-mediated nucleation and autocatalytic growth of nanoparticles,[27] whereas Lazzari et al. reported a kinetic study of ligand-mediated CdSe nanoparticle formation. The authors fit their model to the experimental data and extracted temperature-dependent kinetic parameters.[28]

We adapted the method of Lazzari et al.[28] and developed a ligand-mediated model of NC formation in which we investigate the parameter space of NC formation. We explore the initial conditions and rate constants that allow the synthesis of stable S-NCs and NCs. Our kinetic model involves a precursor conversion of ions to neutral atoms associated to ligands and then formation of dimer nuclei followed by ligand-mediated growth through ligand-associated monomer addition and autocatalytic surface growth of seed clusters. We derived kinetic equations for our model and solved them numerically using an ordinary differential equation (ODE) solver in MATLAB. We do not model diffusion and assume that NC formation is controlled by the reaction kinetics of the homogenously mixed solution. Experimentally, rapid mixing

Received: August 13, 2019
Revised: October 11, 2019
Published: November 5, 2019

DOI: 10.1021/acs.jpcc.9b07683
J. Phys. Chem. C 2019, 123, 29954−29963

of reagents can be achieved with micromixers.[29] We use the model to predict the size distributions of NCs for a range of kinetic parameters, starting conditions, and reaction schemes.

The kinetic model explicitly shows the important role of ligands in NC nucleation and growth. The NC size distribution shifts to larger sizes with increasing ligand-associated monomer growth or autocatalytic surface growth rates. The model confirms that fast nucleation forms small clusters. A high rate of monomer formation, rapid association of ligand with metal ion/atom, and fast nucleation results in S-NCs. We show that rapidly binding ligands kinetically stabilize NCs for both strong and weak reducing agents.[19,29] However, we find that fast autocatalytic growth occurs with a weak reducing agent. Consequently, large (>1.5 nm) polydisperse NCs are formed. In contrast, autocatalytic growth is prevented with a strong reducing agent and stable monodisperse S-NCs are formed. Besides its predictive power, the model provides atomic insight into the mechanism of NC formation, which informs experiments in developing and optimizing methods to produce monodisperse NCs stabilized at early stages of growth in a homogenously mixed solution.

METHODS

The detailed mechanism of the kinetic model is

$$M^+ \xrightarrow{k_{p,1}} M \tag{1a}$$

$$M + L \underset{k_{ub,1}}{\overset{k_{b,1}}{\rightleftharpoons}} ML \tag{1b}$$

$$M^+ + L \underset{k_{ub,2}}{\overset{k_{b,2}}{\rightleftharpoons}} ML^+ \tag{1c}$$

$$ML^+ \xrightarrow{k_{p,2}} ML \tag{1d}$$

$$ML + ML \xrightarrow{k_n} C_{2,2} \tag{1e}$$

$$ML + ML^+ \xrightarrow{k_{n,ac}} C_{2,2} \tag{1f}$$

$$C_{i,j} + ML \underset{k_{d,j+1}}{\overset{k_{g,i,j}}{\rightleftharpoons}} C_{i+1,j+1} \tag{1g}$$

$$C_{i,j} + ML^+ \underset{k_{d,j+1,ac}}{\overset{k_{g,i,j,ac}}{\rightleftharpoons}} C_{i+1,j+1} \tag{1h}$$

$$C_{i,j} + L \underset{k_{e,j+1}}{\overset{k_{a,i,j}}{\rightleftharpoons}} C_{i,j+1} \tag{1i}$$

where the cluster $C_{i,j} = M_iL_j$ is composed of i metal atoms M and j ligands L. The reaction scheme starts with eq 1a representing the reduction of the precursor metal ion (M^+) to zero-valent metal atom (M) with rate constant $k_{p,1}$. Examples of M and M^+ are gold (Au) and silver (Ag) atoms and their corresponding monovalent cations. The precursor and neutral metal atom are typically solvated and coordinated with one or more ligands, for example, thiolate or phosphine. The scheme could reasonably start at eq 1d, but we explicitly consider ligand-binding in our model. Oligomers are excluded from our reaction scheme for the sake of simplicity.

In experiments, the concentration of the reducing agent is often many times the concentration of the metal precursor.[17,19,30−34] For example, Luo et al. used approximately 70 equivalents of carbon monoxide as a reducing agent in the synthesis of gold thiolate NCs.[35] Therefore, we approximate the reduction step 1a as a first-order reaction. Equations 1b and 1c show the ligand binding/unbinding with a metal atom and metal ion to form ML and ML^+ with rate constants $k_{b,1}/k_{ub,1}$ and $k_{b,2}/k_{ub,2}$, respectively. In eq 1d, we account for the conversion of ML^+ to ML with rate constant $k_{p,2}$. Similar to eq 1a, we assume a first-order reaction because of the presence of excess reducing agent.

Equations 1e and 1f illustrate the formation of the neutral dimer $C_{2,2}$ composed of two monomers and two ligands through two pathways: irreversible dimerization of a ligand-associated monomer (ML) with itself (self-dimerization) and with a ligand-associated metal ion (ML^+) (autocatalysis) with rate constants k_n and $k_{n,ac}$, respectively. Equation 1f is actually composed of two steps with a charged dimer intermediate, $ML + ML^+ \rightarrow C_{2,2}^+ \rightarrow C_{2,2}$. Therefore, rate constant $k_{n,ac}$ is an effective rate constant including both steps: ligand-associated ion addition and reduction of the dimer. Charged[29,36,37] and neutral[38] dimers have been detected in the early stages of silver NC formation. Furthermore, experiments indicate that the dimer may be the nuclei for growth and is sometimes referred to as the kinetically effective nucleus.[39] Equations 1g and 1h show that reversible growth occurs through two pathways: addition/dissociation of ML and ML^+ to/from the cluster $C_{i,j}$ to form cluster $C_{i+1,j+1}/C_{i-1,j-1}$ with rate constants $k_{g,i,j}/k_{d,j}$ and $k_{g,i,j,ac}/k_{d,j+1,ac}$ respectively. Equation 1h is also composed of two steps: addition of ligand-associated ion and reduction of the cluster; therefore, $k_{g,ac}$ is an effective rate constant accounting for both steps. Reduction of the positively charged cluster is irreversible but there is a small probability that the ligand-associated ion dissociates from the cluster before reduction occurs. We incorporate this into the scheme above with $k_{d,ac}$. Equation 1i includes reversible ligand association/elimination step of the cluster $C_{i,j}$ to form $C_{i,j+1}$ and $C_{i,j-1}$ with rate constants $k_{a,i,j}$ and $k_{e,j+1}$. These steps outline our kinetic model from which we extract three reaction schemes by modifying the rate coefficients to study NC formation.

For growth of the cluster, the model incorporates the addition of the ligand-associated metal ion (autocatalytic surface growth)[25−27,40−42] and the neutral ligand-associated metal atom (classical growth)[28] to the cluster $C_{i,j}$ to form the cluster $C_{i+1,j+1}$ increasing the number of monomers i and ligands j by one. These two pathways, in addition to coalescent growth,[13,16,18,43] have been extensively discussed in the literature for nanoparticle formation. We did not incorporate coalescent growth into the model because coalescence of large clusters typically occurs on a longer time scale than nucleation[43] and is prevented when ligand-binding is strong. Our interest is in the optimal conditions for the formation of sub-nanometer and nanometer size particles. Furthermore, the kinetic rate equations cannot be solved with the method of moments when ligand-mediated coalescent growth is included. Ligand binding strength and concentration are important factors in kinetically stabilizing S-NCs and NCs in their metastable stages of growth.[17,30−33,44] In this regard, ligand adsorption on the cluster and elimination from it is implemented in the model through which cluster $C_{i,j}$ gains or loses a ligand to form $C_{i,j+1}$ or $C_{i,j-1}$, respectively. Figure 1 presents a schematic of the different ways a cluster $C_{i,j}$ can change its indices i and j and Table 1 lists a summary of the rate coefficients used in the model.

DOI: 10.1021/acs.jpcc.9b07683
J. Phys. Chem. C 2019, 123, 29954−29963

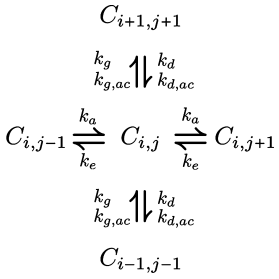

Figure 1. Schematic of the methods by which the clusters can change indices.

Table 1. Rate Coefficients for the Model

reaction	parameter
monomer formation	$k_{p,1}$
ligand binding/unbinding to a metal atom	$k_{b,1}/k_{ub,1}$
ligand binding/unbinding to a metal ion	$k_{b,2}/k_{ub,2}$
reduction of a ligand-associated metal ion	$k_{p,2}$
self dimerization/autocatalytic dimerization	$k_n/k_{n,ac}$
monomer addition growth/dissociation	k_g/k_d
autocatalytic growth/dissociation	$k_{g,ac}/k_{d,ac}$
ligand association/elimination	k_a/k_e

Ligand addition is determined by the number of vacant sites on a cluster of i monomers, whereas ligand elimination is determined by the number of ligands j already occupying those sites. If $N_{s,i}$ is the total number of sites on a cluster with i monomers, the number of vacant sites is $(N_{s,i} - j)$ where j is the number of ligands that are already in occupation. Assuming that the rate coefficients for ligand addition and elimination are linearly dependent on the respective numbers of vacant $(N_{s,i} - j)$ and occupied sites j, we obtain the following

$$k_{g,i,j} = k_g(N_{s,i} - j) \tag{2}$$

$$k_{d,j} = k_d j \tag{3}$$

$$k_{g,i,j,ac} = k_{g,ac}(N_{s,i} - j) \tag{4}$$

$$k_{d,j,ac} = k_{d,ac} j \tag{5}$$

$$k_{a,i,j} = k_a(N_{s,i} - j) \tag{6}$$

$$k_{e,j} = k_e j \tag{7}$$

The number of binding sites on an NC (eq 8) originates from an empirically derived scaling relation for the number of ligands on a cluster with i monomers.[45]

$$N_{s,i} = [2.08i^{2/3}] \tag{8}$$

The brackets in eq 8 round the number to the nearest integer. With this definition for the number of binding sites on an NC, the ratio of the number of metal atoms in the cluster to the number of ligands bound to the cluster, i/j_{max}, increases as a function of i (Figure S1 in the Supporting Information) as expected from the coordination properties of metal atoms. Using the defined rate coefficients (eqs 1a–1i and 2–7), we derived eq 9 for the rate of change of concentration of cluster $C_{i,j}$ with i monomers and j ligands. The minimum and maximum numbers of monomers in eq 9 are $i_{min} = 3$ and $i_{max} = 400$, respectively. The kinetic rate equations for other species M, M^+, L, ML, ML^+, $C_{2,2}$ are listed in the Supporting Information.

$$\begin{aligned}\frac{d}{dt}[C_{i,j}] = &-(k_g[ML] + k_{g,ac}[ML^+])\{[C_{i,j}](N_{s,i} - j) \\ &- [C_{i-1,j-1}](N_{s,i-1} - j + 1)\} \\ &+ (k_d + k_{d,ac})\{[C_{i+1,j+1}](j + 1) - [C_{i,j}]j\} \\ &- k_a[L]\{[C_{i,j}](N_{s,i} - j) - [C_{i,j-1}](N_{s,i} - j + 1)\} \\ &+ k_e\{[C_{i,j+1}](j + 1) - [C_{i,j}]j\}\end{aligned} \tag{9}$$

The rate equations contain two internal coordinates i and j, corresponding to the number of monomers i and ligands j in a cluster $C_{i,j}$. To simplify the equations, we used the method of moments by summing over j to convert each 2-D equation to two 1-D equations.[28] Equations 2–4 define the zeroth, first, and second moments, respectively.

$$[\bar{C}_i] = \sum_{j=0}^{\infty} [C_{i,j}] \tag{10}$$

$$[\bar{L}_i] = \sum_{j=0}^{\infty} j[C_{i,j}] \tag{11}$$

$$[\bar{\bar{L}}_i] = \sum_{j=0}^{\infty} j^2[C_{i,j}] \tag{12}$$

The zeroth moment (eq 10) provides the concentration of clusters with i monomers irrespective of the number of ligands on the surface of the cluster. The first moment (eq 11) calculates the total concentration of ligands on clusters with i monomers. The second moment (eq 12) contains information about the shape of the distribution of ligands on the clusters and can be determined if we further assume that the j ligands are binomially distributed on a cluster with i monomers (eqs 15 and 16), for which there is good experimental evidence.[28,46]

Summing eq 9 over the number of ligands j before and after multiplying by j (eqs 10 and 11), we get two differential equations (eqs 13 and 14) for $[\bar{C}_i(t)]$ and $[L_i(t)]$ with the time dependence suppressed for brevity.

$$\begin{aligned}\frac{d}{dt}[\bar{C}_i] = &-(k_g[ML] + k_{g,ac}[ML^+])\{([\bar{C}_i]N_{s,i} - [\bar{L}_i]) \\ &- ([\bar{C}_{i-1}]N_{s,i-1} - [\bar{L}_{i-1}])\} + (k_d + k_{d,ac})\{[\bar{L}_{i+1}] - [\bar{L}_i]\}\end{aligned} \tag{13}$$

$$\begin{aligned}\frac{d}{dt}[\bar{L}_i] = &-(k_g[ML] + k_{g,ac}[ML^+])\{([\bar{L}_i]N_{s,i} - [\bar{\bar{L}}_i]) \\ &- ([\bar{C}_{i-1}]N_{s,i-1} + [\bar{L}_{i-1}](N_{s,i-1} - 1) - [\bar{\bar{L}}_{i-1}])\} \\ &+ (k_d + k_{d,ac})\{([\bar{\bar{L}}_{i+1}] - [\bar{L}_{i+1}]) - [\bar{\bar{L}}_i]\} \\ &- k_a[L]\{[\bar{C}_i]N_{s,i} - [\bar{L}_i]\} - k_e[\bar{L}_i]\end{aligned} \tag{14}$$

This conversion reduces the number of equations and saves computing time in solving them numerically. To perform the sum, we assume that the number of ligands bound to a cluster with i monomers follows a binomial distribution

DOI: 10.1021/acs.jpcc.9b07683
J. Phys. Chem. C 2019, 123, 29954–29963

Table 2. Rate Coefficients Used to Create Schemes 123

parameters	Scheme 1, classical	Scheme 2, autocatalytic	Scheme 3, combination
$k_{p,1}/k_{p,2}$	1×10^3 $s^{-1}/0$	1×10^{-4} $s^{-1}/1 \times 10^{-3}$ s^{-1}	1×10^3, 1×10^{-4} $s^{-1}/1 \times 10^{-3}$ s^{-1}
$k_{b,1}/k_{ub,1}$	1×10^5 M^{-1} $s^{-1}/1 \times 10^{-7}$ s^{-1}	1×10^5 M^{-1} $s^{-1}/1 \times 10^{-7}$ s^{-1}	1×10^5 M^{-1} $s^{-1}/1 \times 10^{-7}$ s^{-1}
$k_{b,2}/k_{ub,2}$	0/0	1×10^5 M^{-1} $s^{-1}/1 \times 10^{-7}$ s^{-1}	1×10^5 M^{-1} $s^{-1}/1 \times 10^{-7}$ s^{-1}
k_n	1×10^1, 1×10^2, 1×10^3 M^{-1} s^{-1}	0	1×10^2 M^{-1} s^{-1}
$k_{n,ac}$	0	1×10^1, 1×10^2, 1×10^3 M^{-1} s^{-1}	1×10^2 M^{-1} s^{-1}
k_g/k_d	1×10^2 to 1×10^4 M^{-1} $s^{-1}/1 \times 10^{-9}$ s^{-1}	0/0	1×10^2 to 1×10^4 M^{-1} $s^{-1}/1 \times 10^{-9}$ s^{-1}
$k_{g,ac}/k_{d,ac}$	0/0	1×10^2 to 1×10^4 M^{-1} $s^{-1}/1 \times 10^{-9}$ s^{-1}	1×10^2 to 1×10^4 M^{-1} $s^{-1}/1 \times 10^{-9}$ s^{-1}
k_a/k_e	1×10^{-3}, 1×10^6 M^{-1} $s^{-1}/1 \times 10^3$ s^{-1}	1×10^{-3}, 1×10^6 M^{-1} $s^{-1}/1 \times 10^3$ s^{-1}	1×10^{-3}, 1×10^6 M^{-1} $s^{-1}/1 \times 10^3$ s^{-1}

$$p(j|i) = \binom{N_{s,i}}{j} p_i^j (1 - p_i)^{N_{s,i}-j} \tag{15}$$

where p_i is the probability of finding a bound ligand with respect to the total number of available sites ($N_{s,i}$) on a cluster with i monomers.[45]

$$p_i = \frac{[\bar{L}_i]}{[\bar{C}_i]N_{s,i}} \tag{16}$$

The concentration of clusters with i monomers and j ligands is then

$$[C_{i,j}] = [\bar{C}_i]p(j|i) \tag{17}$$

Finally, eq 18 is obtained with the assumption of binomially distributed ligands on the clusters.[28,46]

$$[\bar{\bar{L}}_i] = \sum_{j=0}^{\infty} j^2 [C_{i,j}] = [\bar{L}_i](1 - p_i + N_{s,i}p_i) \tag{18}$$

The coupled ODEs were solved numerically using ode15s in MATLAB. The solution to the kinetic rate equations provides the population of clusters $[\bar{C}_i(t)]$ with i monomers as a function of time. Using a method described elsewhere, the monomeric distribution of clusters is transformed to a size distribution using eq 19, where D_M = 0.25 nm is the monomer diameter.[28] The factor 0.45 originates from a scaling relation between the dimensionless mass of the clusters (i) and the clusters' diameter.[28]

$$C_D(t) = 3\frac{0.45^{1/3}}{D_M} i^{2/3} C_i(t) \tag{19}$$

Table 1 presents the rate coefficients used in our model, and Table 2 displays reasonable magnitudes for three reaction schemes that are discussed in the Results and Discussion.

RESULTS AND DISCUSSION

To understand the role of ligands in stabilizing NCs, we developed a ligand-mediated kinetic model in which growth is governed by ligand-associated monomer addition to the cluster and autocatalytic surface growth (see Methods). Experiments indicate that an excess of ligand, for example, thiolates[47,48] or phosphines,[49,50] can shift the NC size distribution to smaller sizes and may trap NCs in their early stages of growth.[17,30−33] Inspired by these experiments, our reaction schemes utilize a large ligand to metal ion molar ratio of 6.00 mM/0.05 mM = 120.

We investigated four reaction schemes. Scheme 1 (Table 2) has the rate coefficients associated with autocatalytic growth ($k_{b,2}$, $k_{ub,2}$, k_{p2}, $k_{n,ac}$, $k_{g,ac}$, $k_{d,ac}$) set to zero and utilizes a strong reducing agent ($k_{p,1}$ = 10^3 s^{-1}) to induce fast nucleation.

Scheme 1. Ligand-Mediated Classical Growth

$$M^+ \xrightarrow{k_{p,1}} M$$
$$M + L \underset{k_{ub,1}}{\overset{k_{b,1}}{\rightleftharpoons}} ML$$
$$ML + ML \xrightarrow{k_n} C_{2,2}$$
$$C_{i,j} + ML \underset{k_{d,i,j}}{\overset{k_{g,i,j}}{\rightleftharpoons}} C_{i+1,j+1}$$
$$C_{i,j} + L \underset{k_{e,i,j}}{\overset{k_{a,i,j}}{\rightleftharpoons}} C_{i,j+1}$$

Scheme 1 conforms to the classical LaMer growth mechanism. On the other hand, Scheme 2 (Table 2) has the rate constants for ligand-associated monomer nucleation k_n, growth k_g, and dissociation k_d set to zero and utilizes a weak reducing agent ($k_{p,1}$ = 10^{-4} s^{-1}, $k_{p,2}$ = 10^{-3} s^{-1}), to induce slow, continuous nucleation. Scheme 2 conforms to the autocatalytic growth mechanism. Scheme 3 combines both ligand-associated monomer nucleation and growth with autocatalytic growth

Scheme 2. Autocatalytic Surface Growth

$$M^+ \xrightarrow{k_{p,1}} M$$
$$M + L \underset{k_{ub,1}}{\overset{k_{b,1}}{\rightleftharpoons}} ML$$
$$M^+ + L \underset{k_{ub,2}}{\overset{k_{b,2}}{\rightleftharpoons}} ML^+$$
$$ML^+ \xrightarrow{k_{p,2}} ML$$
$$ML + ML^+ \xrightarrow{k_{n,ac}} C_{2,2}$$
$$C_{i,j} + ML^+ \underset{k_{d,i,j,ac}}{\overset{k_{g,i,j,ac}}{\rightleftharpoons}} C_{i+1,j+1}$$
$$C_{i,j} + L \underset{k_{e,i,j}}{\overset{k_{a,i,j}}{\rightleftharpoons}} C_{i,j+1}$$

Scheme 3. Ligand-Associated Monomer-Addition and Autocatalytic Surface Growth

$$M^+ \xrightarrow{k_{p,1}} M$$
$$M + L \underset{k_{ub,1}}{\overset{k_{b,1}}{\rightleftharpoons}} ML$$
$$M^+ + L \underset{k_{ub,2}}{\overset{k_{b,2}}{\rightleftharpoons}} ML^+$$
$$ML^+ \xrightarrow{k_{p,2}} ML$$
$$ML + ML \xrightarrow{k_n} C_{2,2}$$
$$ML + ML^+ \xrightarrow{k_{n,ac}} C_{2,2}$$
$$C_{i,j} + ML \underset{k_{d,i,j}}{\overset{k_{g,i,j}}{\rightleftharpoons}} C_{i+1,j+1}$$
$$C_{i,j} + ML^+ \underset{k_{d,i,j,ac}}{\overset{k_{g,i,j,ac}}{\rightleftharpoons}} C_{i+1,j+1}$$
$$C_{i,j} + L \underset{k_{e,i,j}}{\overset{k_{a,i,j}}{\rightleftharpoons}} C_{i,j+1}$$

DOI: 10.1021/acs.jpcc.9b07683
J. Phys. Chem. C 2019, 123, 29954−29963

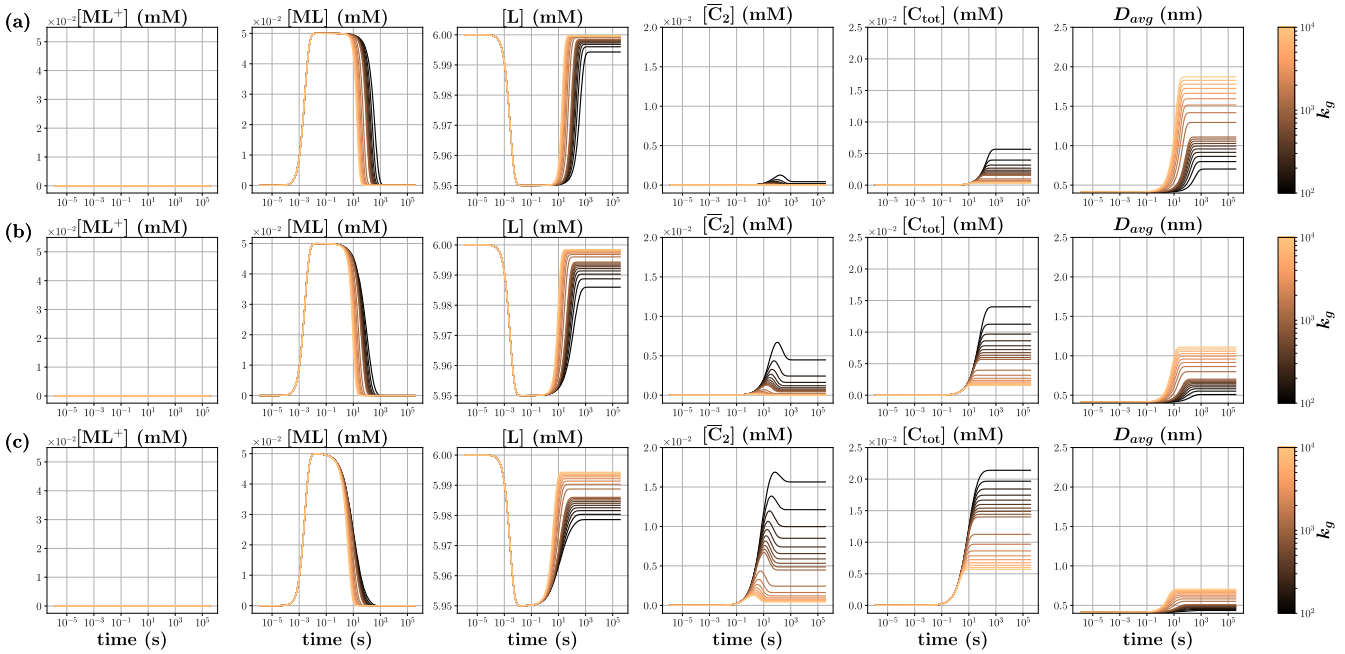

Figure 2. Scheme 1 time evolution of $[ML^+]$, [ML], [L], $[\overline{C}_2]$, $[C_{tot}]$, and average diameter D_{avg} for different ligand-associated monomer growth and self-dimerization rate coefficients (k_g, k_n). Each graph contains plots for 18 different growth rate coefficients k_g from 10^2 to 10^4 M^{-1} s^{-1}, distinguished by colors. Each row is plotted for different dimerization rate coefficients k_n (a) 10^1, (b) 10^2, and (c) 10^3 M^{-1} s^{-1}. The initial concentrations were [L] = 6.00 mM and $[M^+]$ = 0.05 mM.

to investigate the predominance of each NC formation mechanism. Finally, Scheme 4 incorporates NC growth through the addition of a bare metal atom/ion. These calculations were done as a check on our assumption that NCs without adsorbed ligands will experience uncontrolled growth. The results show that when the ligand binding and association rates are smaller than the growth rate, the NCs grow to large sizes as the growth rate increases (Figure S4). In experiments which demonstrate NC synthesis, the metal is already bound to one or more ligands before the solution is mixed with a reducing agent. Accordingly, in Schemes 1, 2, and 3 we set the ligand binding rate to a value (10^5 M^{-1} s^{-1}) larger than the maximum growth rate (see Table 2). Scheme 3 results for smaller values of k_b are in the Supporting Information (Figures S3 and S4) and we find that the size distributions are nearly indistinguishable from the distributions obtained with k_b = 10^5 M^{-1} s^{-1}.

Schemes 1, 2, and 3 show that the smallest NCs are obtained with fast dimerization (nucleation) and slow growth in the presence of a rapidly binding ligand. The rapidly binding ligands act as a barrier for growth. We elaborate on this observation by calculating the probability of an NC with 10 monomers having ligands on its surface with slowly and rapidly binding ligands. Scheme 3 shows that a strong reducing agent results in small NCs as it promotes fast monomer formation and nucleation,[51] which we observe favors classical growth over autocatalytic growth. Conversely, with a weak reducing agent, monomer formation occurs slowly while many charged monomers are available for autocatalytic growth. As a result, the NCs have larger diameters compared to the results with a strong reducing agent in Scheme 3.

Scheme 1. We investigated ligand-mediated single monomer (classical) growth by setting the autocatalytic growth rates ($k_{b,2}$, $k_{ub,2}$, k_{p2}, $k_{n,ac}$, $k_{g,ac}$, $k_{d,ac}$) to zero and observing the model's results with physically reasonable values of $k_{p,1}$, k_n, k_g, and k_a. Table 2 lists the rate constants used for this reaction scheme. We could not observe NC growth without a large ligand elimination rate k_e. First, we discuss results for a small ligand association rate k_a (10^{-3} M^{-1} s^{-1}), assuring that the NCs have a bare surface. These results are contrasted with a large ligand association rate (10^6 M^{-1} s^{-1}) providing NCs with surfaces covered in ligands.

Figure 2 displays the time evolution of different species, including $[ML^+]$, [ML], [L], $[\overline{C}_2]$, the total concentration of clusters $[C_{tot}]$, and the average diameter D_{avg} (nm) of NCs for different k_n and k_g. Each of the reactants equilibrate within 1000 seconds for all combinations of k_g and k_n used in Figure 1. $[ML^+]$ remains zero through time because the autocatalytic rate constants are set to zero. [ML] increases to a flat maximum value of 0.05 mM being produced by the M + L step and is consumed completely through self-dimerization and single monomer growth. Conversely, 6.00 mM L decreases to a flat minimum of 5.95 mM after completely associating with 0.05 mM M. [L] then increases during NC growth before finally reaching an equilibrium concentration. The dimer concentration $[\overline{C}_2]$ passes through a maximum before reaching a solubility concentration, displaying the classical LaMer curve.[21,22] The concentration of total clusters $[C_{tot}]$ and the average diameter D_{avg} increase in time up to equilibration time. Figure 2a–c shows that the average diameter D_{avg} of NCs grows larger with an increase of k_g and decreases with an increase of k_n. As the rate coefficient k_n increases, more dimers are produced, providing more nuclei for growth. Consequently, the NCs have a smaller average diameter once growth is complete. The number of ligands released during growth also displays a sensitive dependence on the rate coefficient k_g and k_n. As k_g increases, more ligands must be released from the NC surface for growth to occur. Therefore, the equilibrium concentration of L increases with an increase in growth rate

DOI: 10.1021/acs.jpcc.9b07683
J. Phys. Chem. C 2019, 123, 29954−29963

k_g. Conversely, the number of free ligands decreases with an increase in k_n because more dimers form.

The results of Figure 2 were calculated with a ligand association rate coefficient of $k_a = 10^{-3}$ M^{-1} s^{-1}. We also investigated the dependence of NC sizes on k_g and k_n with a large ligand association rate constant ($k_a = 10^6$ M^{-1} s^{-1}). Small and large k_a correspond to slowly and rapidly binding ligands, respectively. Figure 3a again indicates increasing k_n results in smaller NCs, as discussed in Figure 2. Figure 3c displays the NC size distribution for $k_a = 10^6$ M^{-1} s^{-1}. For the same rate constants k_g and k_n, rapidly binding ligands form smaller NCs. Figure 3b shows that increasing the growth rate k_g with a slowly binding ligand shifts the size distribution to larger NCs. In contrast, Figure 3d displays the NC size distribution obtained with a rapidly binding ligand for increasing k_g. With a rapidly binding ligand, the NCs do not grow significantly with an increase in k_g by two factors of 10. This trend reflects the limited number of binding sites on the surface of the NCs.

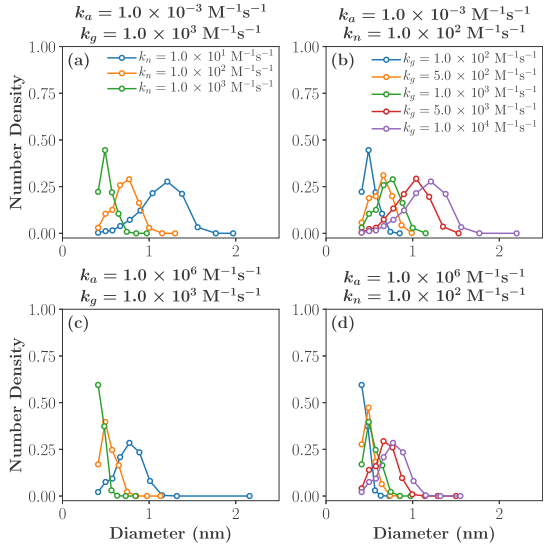

Figure 3. Scheme 1 shift of size distribution to smaller clusters with an increase of ligand association rate constant from (a) 10^{-3} to (c) 10^6 M^{-1} s^{-1} for different self-dimerization rates k_n. (b) and (d) Shift of size distribution to smaller clusters with an increase of the ligand association rate for different growth rates k_g. The initial concentrations were $[M^+]$ = 0.05 mM and [L] = 6.00 mM.

Scheme 2. Autocatalytic surface growth involves the addition of a charged monomer (ML^+) to the growing NC, while simultaneously being reduced. Therefore, we set the neutral monomer (ML) dimerization k_n and growth and dissociation rate constants k_g and k_d equal to zero, which provides a model for ligand-mediated autocatalytic NC formation. Table 1 lists the rate constants used for this reaction scheme.

Similar to Figure 2, Figure 4 shows the trend of decreasing average NC diameter for increasing dimerization rate. ML^+ is formed through M^+ + L and reaches a maximum of approximately 0.05 mM and then is consumed through autocatalytic growth and conversion to ML. Formation of ML mostly occurs through the reduction of ML^+, but as $k_{n,ac}$ increases from 10^1 to 10^3 M^{-1} s^{-1} the equilibrium concentration of ML decreases. Figure 4 also shows $[\bar{C}_2]$ evolution with no transient maximum, which implies that autocatalytic dimerization no longer conforms to the classical LaMer paradigm in this case.

Like Scheme 1, we studied the effect of $k_{n,ac}$ and $k_{g,ac}$ on the NC size distribution. Figure 5a,b presents the trend in NC size distribution for different (a) $k_{n,ac}$ and (b) $k_{g,ac}$. Fast dimerization results in relatively smaller NCs, whereas fast growth forms relatively larger NCs in the presence of slowly

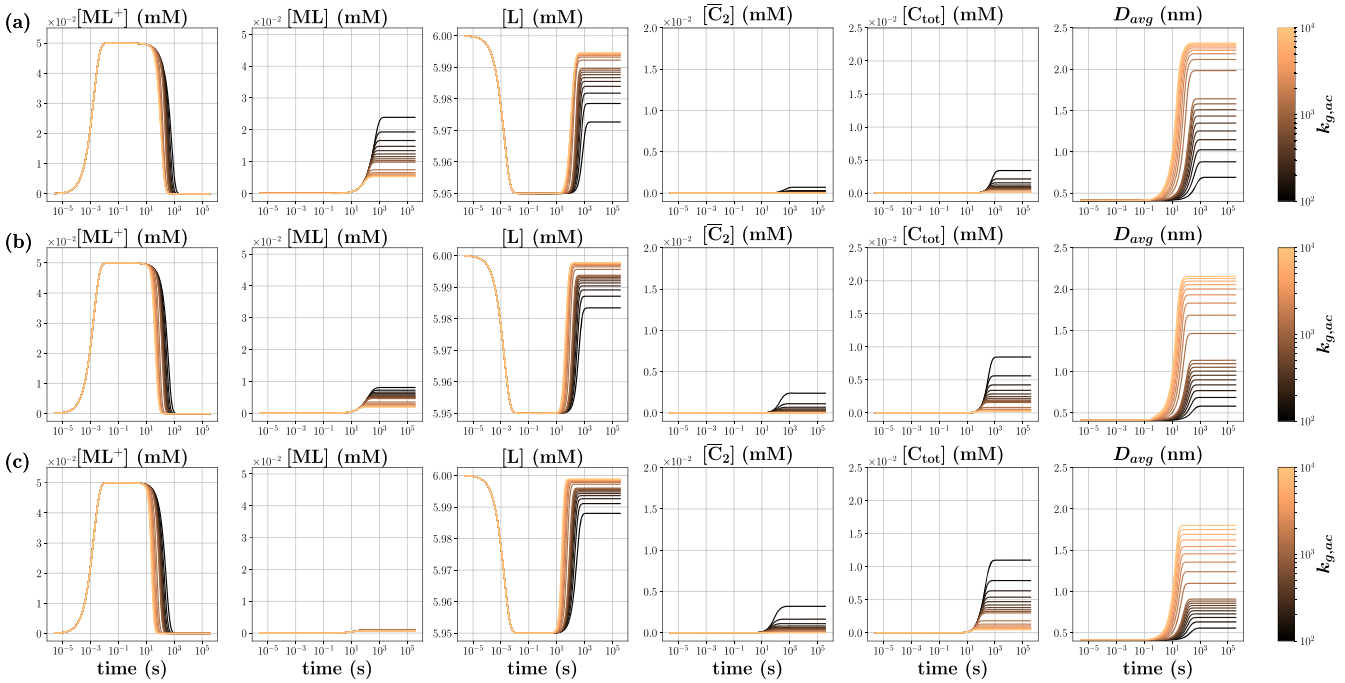

Figure 4. Time evolution of $[ML^+]$, [ML], [L], $[\bar{C}_2]$, $[C_{tot}]$, and average diameter D_{avg} for different autocatalytic growth and dimerization rate coefficients ($k_{g,ac}$, $k_{n,ac}$) in a reaction between 6.00 mM L and 0.05 mM M^+. Each graph contains plots for 18 different $k_{g,ac}$ from 10^2 to 10^4 M^{-1} s^{-1} distinguished by colors. Each row is plotted for different $k_{n,ac}$ (a) 10^1, (b) 10^2, and (c) 10^3 M^{-1}.

DOI: 10.1021/acs.jpcc.9b07683
J. Phys. Chem. C 2019, 123, 29954−29963

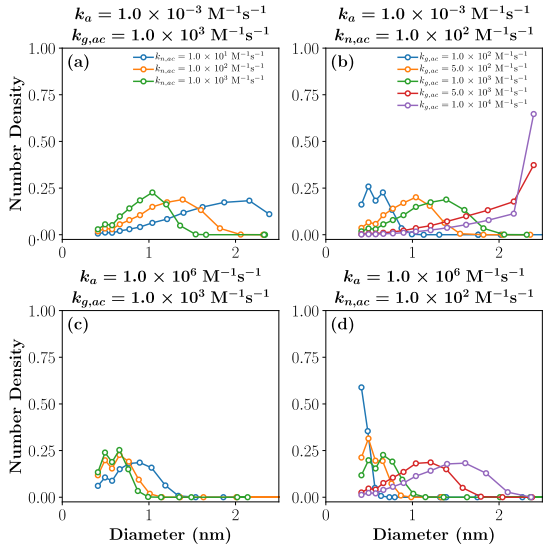

Figure 5. Scheme 2 shift of size distribution to smaller clusters with an increase in ligand association rate from (a) 10^{-3} to (c) 10^{6} for different autocatalytic dimerization rates $k_{n,ac}$. (b) and (d) Shift of size distribution to smaller clusters with an increase of the ligand association rate for different autocatalytic growth rates $k_{g,ac}$. The initial concentrations were $[M^+]$ = 0.05 mM and [L] = 6.00 mM.

binding ligands. With a rapidly binding ligand (Figure 5c,d), the NCs have smaller average diameters for the same k_n and k_g in comparison to slowly binding ligands. Similar to Scheme 1, this implies that rapidly binding ligands inhibit NC growth and trap them in early metastable stages of growth. Again, this observation is a reflection of the limited number of binding sites on the surface of an NC. In comparison to Scheme 1 and Figure 3, it is apparent that the average NC diameter is larger when a weak reducing agent is used. Furthermore, the size distribution of NCs is broadened (Figure 5) in comparison to the single monomer growth pathway with a strong reducing agent (Figure 3).

Scheme 3. In this scheme, both neutral monomer (ML) addition and autocatalytic growth pathways are active, which is a more likely scenario in real systems.[29,37] Table 2 lists the rate constants used for Scheme 3. In the presence of a strong reducing agent, many neutral monomers are produced. Consequently, many nuclei (dimers) are available for growth and the average diameter of NCs is relatively small. However, in the presence of a weak reducing agent, fewer neutral monomers are produced but many charged monomers are available for autocatalytic growth. Therefore, in the presence of a weak reducing agent, the average diameter of NCs is expected to be large. In light of this, we investigated the effect of $k_{p,1}$ as a switch between classical and autocatalytic growth. Classical growth predominates with large $k_{p,1}$ (strong reducing agent). Conversely, autocatalytic growth predominates with small $k_{p,1}$ (weak reducing agent).

Figure 6a,b shows the time-dependent concentration of different species from Scheme 3 for (a) $k_{p,1} = 10^{3}$ s^{-1} and (b) $k_{p,1} = 10^{-4}$ s^{-1}. Similar trends to Figure 2 are observed in Figure 6a, despite the presence of the autocatalytic growth pathway in Figure 6a. Specifically, ML shows a similar time dependence in both plots. Furthermore, $[\bar{C}_2]$ has regained the LaMer shape, which was not present in Figure 4 with autocatalytic growth. Similar to Figure 4, Figure 6b shows a delay in the production of ML. However, ML abruptly decreases in concentration in Figure 6b because of the presence of the classical growth pathway. Comparing Figure 6a,b, it is evident that classical nucleation and growth predominates in the presence of a strong reducing agent, and autocatalytic growth predominates with a weak reducing agent. Furthermore, the average diameter D_{avg} of NCs is smaller with a strong reducing agent, which we suggest is due to the presence of more nuclei.

To elaborate on the contrasting results obtained with strong and weak reducing agents for Scheme 3, we also discuss the effects of changing the concentration of the metal ion precursor (M^+) and the ligand association rate to the NCs. Similar to Schemes 1 and 2, we observe smaller NCs in the presence of a rapidly binding ligand. Figure 7b,d show that NCs with diameters less than 1 nm can be obtained with a strong or weak reducing agent in the presence of a rapidly binding ligand.[19] However, when a weak reducing agent is used, the NCs are more sensitive to an increase in concentration of the metal ion precursor and the average diameter shifts to larger sizes as the concentration increases (Figure 7c,d). Figure 7a,b indicates that the concentration of the metal ion does not affect the NC size distribution using a strong reducing agent, which is likely due to the lack of NC

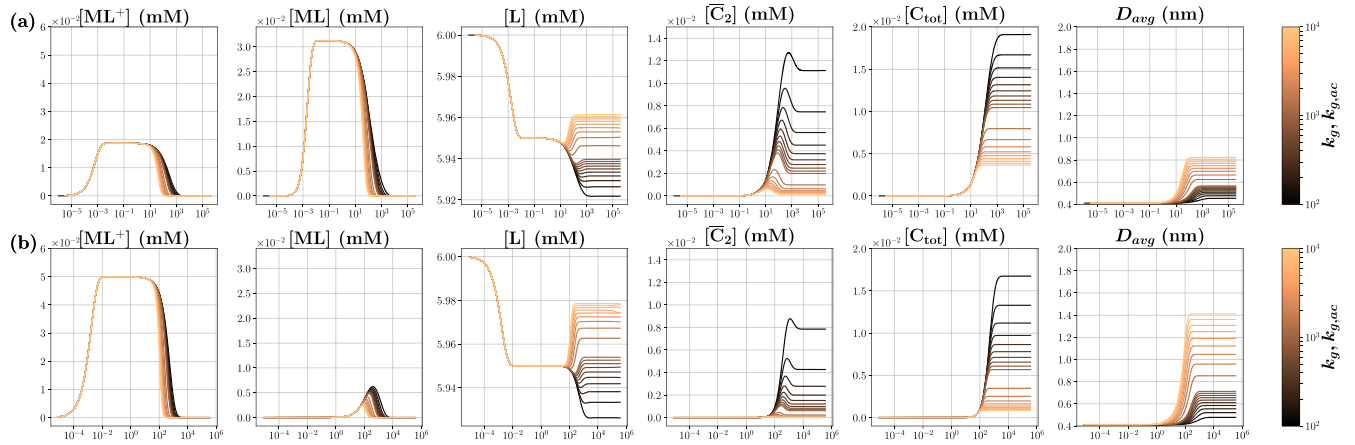

Figure 6. Scheme 3 time evolution of $[ML^+]$, [ML], [L], $[\bar{C}2]$, $[C_{tot}]$, and average diameter D_{avg} with different growth and rates (k_g, $k_{g,ac}$, $k_{p,1}$) for $k_{p,1}$ (a) 10^{3}, (b) 10^{-4} s^{-1}. Each graph contains plots for 18 different k_g and $k_{g,ac}$ from 10^{2} to 10^{4} M^{-1} s^{-1} distinguished by colors. The initial concentrations are 6.00 mM L and 0.05 mM M^+.

DOI: 10.1021/acs.jpcc.9b07683
J. Phys. Chem. C 2019, 123, 29954−29963

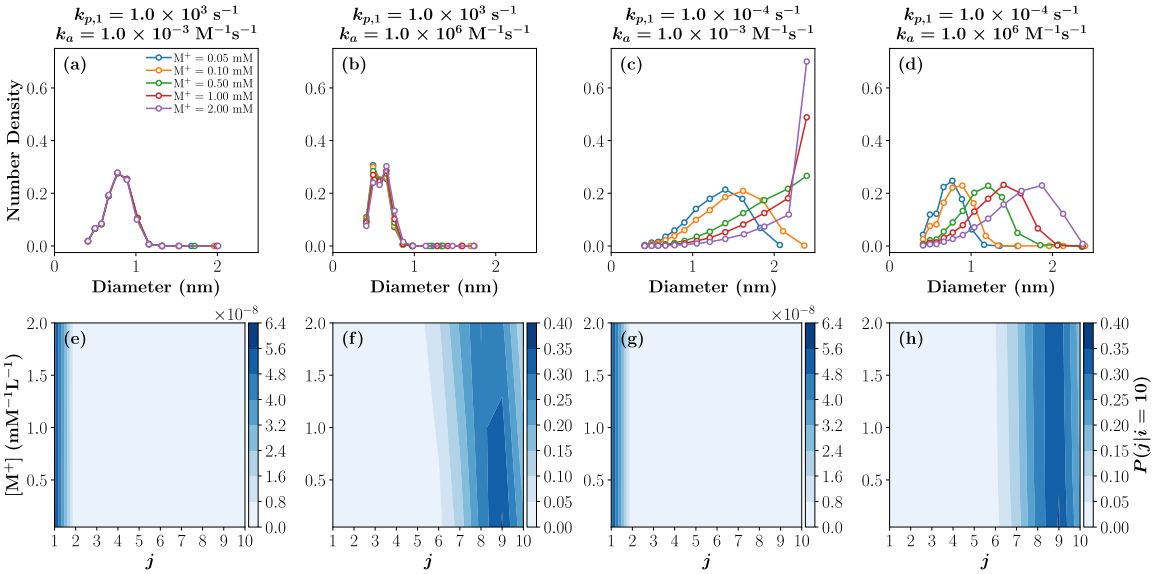

Figure 7. Scheme 3 (a–d) NC size distribution for different concentrations of M^+ and L using a fast or a slow reducing agent in the presence of a strong or a weak ligand. (e-h) Probability of finding j number of ligands on an NC given i = 10 corresponding to the rates in (a–d), respectively.

growth through the addition of a non-ligand-associated metal atom in our model.

To illustrate the effect of ligand association rate to the NC, Figure 7e–h shows the probability of finding j ligands on the surface of the $M_{10}L_j$ NC with a diameter near 0.7 nm. Figure 7e,g indicates that the probability of finding a single ligand on the surface of clusters with 10 monomers is approximately zero. On the other hand, Figure 7f,h shows that 100% of NCs with 10 monomers have more than 5 ligands on their surface. Furthermore, 40% of NCs with 10 monomers have 9 of the possible 10 binding sites covered in ligands. These observations emphasize the role of ligands in occupying binding sites on the NC surface and thereby inhibiting NC growth.

As an example, we compare the results of our calculations to experimental results obtained through radiolytic reduction of metal ions in solution. Belloni et al.[29] used gamma-radiation to produce solvated electrons and free radicals, which then reduced monovalent silver atoms in solution and induced silver NC nucleation and growth. The researchers observed smaller metal clusters at high radiation dose rates compared to low radiation dose rates. At high dose rates, most of the ions were reduced to neutral monomers in solution, providing many nuclei for growth. At low rates, relatively few neutral monomers were produced, but many monovalent metal atoms were available for autocatalytic growth, resulting in larger nanoparticles. Our model supports these findings and illustrates the NC sizes that could be obtained using a chemical reducing agent in solution (Figures 6 and 7). In this case, we emphasize that microfluidic mixers may be needed to ensure fast mixing of reactants.

As a second example, we compare the model to recent experiments on gold thiolate NCs produced through gold precursor reduction by carbon monoxide, which show a contrasting trend[51] to the trend presented here. The reduction kinetics of carbon monoxide was modified by adjusting the pH of the solution. At pH 11, the reduction kinetics of carbon monoxide is faster than at pH 7. The researchers observed larger NCs ($M_{25}L_{18}$) with faster reduction kinetics at pH 11 than at pH 7 ($M_{10-12}L_{10-12}$).[52] Our model would suggest that the opposite trend should be observed where smaller clusters are obtained with faster reduction kinetics because more nuclei are produced. To clarify the contrasting observations, we point out that gold thiolate forms oligomers in solution, and the size of the oligomer species is pH-dependent with smaller structures observed at a higher pH.[53] In other words, more gold thiolate nuclei are present at higher pH and thus smaller NCs are obtained after growth completes.[53] Our model does not incorporate the formation of oligomeric structures, but it is qualitatively consistent with the observation that a greater number of nuclei produce smaller NCs.

In summary, the model shows that fast nucleation, slow growth, high molar ratio of rapidly binding ligand to metal ion in a well-mixed solution promotes the formation of small NCs. Examples are the formation of gold and silver NCs and sub-NCs (S-NCs) in mixing experiments. The use of microfluidic devices could provide well-mixed solutions to facilitate NC formation.[54−59] Finally, the model can be improved by incorporation of coalescent growth, diffusion, and kernels (rate constants) that account for the interaction between species in the system (e.g., DLVO theory).[18,33] The model could be extended by incorporating metal atoms that bind to more than one ligand, for example, ML_2 or ML_3. Our model would predict that smaller NCs would be obtained in comparison to growth through ML as fewer surface sites would be available for growth if more than one ligand were bound to the metal monomer. This prediction is observed in experiments.[60]

■ CONCLUSIONS

We combined ligand-mediated monomer addition and autocatalytic surface growth in a kinetic model to understand the mechanism of NC formation, which, to our knowledge, is the first study to do so. Our detailed investigation explicitly showed that fast nucleation and slow growth promotes the formation of small NCs. Our results suggest that even with a slow reducing agent, the NCs can be kinetically stabilized by ligands binding to the NC surfaces. This implies that ligands stabilize and facilitate the formation of NCs by suppressing growth and isolating NCs in their metastable states. Finally, the

DOI: 10.1021/acs.jpcc.9b07683
J. Phys. Chem. C 2019, 123, 29954−29963

kinetic model showed that, in a well-mixed solution, a high molar ratio of ligand to metal, for example, 6.00 mM/0.05 mM = 120, inhibits growth and promotes the stabilization of small NCs.

■ ASSOCIATED CONTENT

Supporting Information

The Supporting Information is available free of charge at https://pubs.acs.org/doi/10.1021/acs.jpcc.9b07683.

Additional equations, details about the methods, Scheme 3 results for $k_b = 10^2$, and 10^3 M^{-1} s^{-1}, and Scheme 4 with size distributions for various combinations of k_b and k_a (PDF)

■ AUTHOR INFORMATION

Corresponding Author

*E-mail: rasaiah@maine.edu.

ORCID

Mohsen Farshad: 0000-0001-5095-4361

Dylan Suvlu: 0000-0003-3216-1338

Jayendran C. Rasaiah: 0000-0002-4453-7438

Author Contributions

M.F. and D.S. contributed equally. The paper was written through contributions of all the authors. All the authors have given approval to the final version of the paper.

Notes

The authors declare no competing financial interest.

■ ACKNOWLEDGMENTS

The authors acknowledge Stefano Lazzari and Klavs Jensen for correspondence. The authors thank Attila Szabo for helpful comments. The authors are grateful for supercomputer time provided by the Advanced Computing Group at the University of Maine and in particular Steven Cousins for his continuous support.

■ ABBREVIATIONS

NC, nanocluster; S-NC, sub-nanometer cluster; CNT, classical nucleation theory; ODE, ordinary differential equation; FW, Finke–Watzky

■ REFERENCES

(1) Lu, Y.; Chen, W. Sub-Nanometre Sized Metal Clusters: From Synthetic Challenges to the Unique Property Discoveries. *Chem. Soc. Rev.* **2012**, *41*, 3594.

(2) Chakraborty, I.; Pradeep, T. Atomically Precise Clusters of Noble Metals: Emerging Link Between Atoms and Nanoparticles. *Chem. Rev.* **2017**, *117*, 8208–8271.

(3) Jin, R.; Zeng, C.; Zhou, M.; Chen, Y. Atomically Precise Colloidal Metal Nanoclusters and Nanoparticles: Fundamentals and Opportunities. *Chem. Rev.* **2016**, *116*, 10346–10413.

(4) Liu, L.; Corma, A. Metal Catalysts for Heterogeneous Catalysis: From Single Atoms to Nanoclusters and Nanoparticles. *Chem. Rev.* **2018**, *118*, 4981–5079.

(5) Zhao, S.; Jin, R.; Jin, R. Opportunities and Challenges in CO2 Reduction by Gold- And Silver-Based Electrocatalysts: From Bulk Metals To Nanoparticles And Atomically Precise Nanoclusters. *ACS Energy Lett.* **2018**, *3*, 452–462.

(6) Fang, J.; Zhang, B.; Yao, Q.; Yang, Y.; Xie, J.; Yan, N. Recent Advances in The Synthesis and Catalytic Applications of Ligand-Protected, Atomically Precise Metal Nanoclusters. *Coord. Chem. Rev.* **2016**, *322*, 1–29.

(7) Tao, Y.; Li, M.; Ren, J.; Qu, X. Metal Nanoclusters: Novel Probes for Diagnostic and Therapeutic Applications. *Chem. Soc. Rev.* **2015**, *44*, 8636–8663.

(8) Zhang, L.; Wang, E. Metal Nanoclusters: New Fluorescent Probes for Sensors and Bioimaging. *Nano Today* **2014**, *9*, 132–157.

(9) Shang, L.; Dong, S.; Nienhaus, G. U. Ultra-Small Fluorescent Metal Nanoclusters: Synthesis and Biological Applications. *Nano Today* **2011**, *6*, 401–418.

(10) Lee, T.-H.; Gonzalez, J. I.; Zheng, J.; Dickson, R. M. Single-Molecule Optoelectronics. *Acc. Chem. Res.* **2005**, *38*, 534–541.

(11) Webb, J. A.; Bardhan, R. Emerging Advances in Nanomedicine with Engineered Gold Nanostructures. *Nanoscale* **2014**, *6*, 2502.

(12) Jin, R.; Qian, H.; Wu, Z.; Zhu, Y.; Zhu, M.; Mohanty, A.; Garg, N. Size Focusing: A Methodology for Synthesizing Atomically Precise Gold Nanoclusters. *J. Phys. Chem. Lett.* **2010**, *1*, 2903–2910.

(13) Zheng, H.; Smith, R. K.; Jun, Y.-w.; Kisielowski, C.; Dahmen, U.; Alivisatos, A. P. Observation of Single Colloidal Platinum Nanocrystal Growth Trajectories. *Science* **2009**, *324*, 1309–1312.

(14) Rempel, J. Y.; Bawendi, M. G.; Jensen, K. F. Insights into the Kinetics of Semiconductor Nanocrystal Nucleation and Growth. *J. Am. Chem. Soc.* **2009**, *131*, 4479–4489.

(15) Watzky, M. A.; Finke, R. G. Gold Nanoparticle Formation Kinetics and Mechanism: A Critical Analysis of the "Redox Crystallization" Mechanism. *ACS Omega* **2018**, *3*, 1555–1563.

(16) Takesue, M.; Tomura, T.; Yamada, M.; Hata, K.; Kuwamoto, S.; Yonezawa, T. Size of Elementary Clusters and Process Period in Silver Nanoparticle Formation. *J. Am. Chem. Soc.* **2011**, *133*, 14164–14167.

(17) Wuithschick, M.; Paul, B.; Bienert, R.; Sarfraz, A.; Vainio, U.; Sztucki, M.; Kraehnert, R.; Strasser, P.; Rademann, K.; Emmerling, F.; Polte, J. Size-Controlled Synthesis of Colloidal Silver Nanoparticles Based on Mechanistic Understanding. *Chem. Mater.* **2013**, *25*, 4679–4689.

(18) Polte, J. Fundamental Growth Principles of Colloidal Metal Nanoparticles – A New Perspective. *CrystEngComm* **2015**, *17*, 6809–6830.

(19) Nasaruddin, R. R.; Chen, T.; Yan, N.; Xie, J. Roles of Thiolate Ligands in The Synthesis, Properties and Catalytic Application of Gold Nanoclusters. *Coord. Chem. Rev.* **2018**, *368*, 60–79.

(20) Rossi, L. M.; Fiorio, J. L.; Garcia, M. A. S.; Ferraz, C. P. The Role and Fate of Capping Ligands in Colloidally Prepared Metal Nanoparticle Catalysts. *Dalton Trans.* **2018**, *47*, 5889.

(21) LaMer, V. K.; Dinegar, R. H. Theory, Production and Mechanism of Formation of Monodispersed Hydrosols. *J. Am. Chem. Soc.* **1950**, *72*, 4847–4854.

(22) Thanh, N. T. K.; Maclean, N.; Mahiddine, S. Mechanisms of Nucleation and Growth of Nanoparticles in Solution. *Chem. Rev.* **2014**, *114*, 7610–7630.

(23) Becker, R.; Döring, W. Kinetische Behandlung Der Keimbildung in Übersättigten Dämpfen. *Ann. Phys.* **1935**, *416*, 719–752.

(24) Watzky, M. A.; Finke, R. G. Nanocluster Size-Control and "Magic Number" Investigations. Experimental Tests of the "Living-Metal Polymer" Concept and of Mechanism-Based Size-Control Predictions Leading to the Syntheses of Iridium(0) Nanoclusters Centering about Four Sequential Magic Numbers. *Chem. Mater.* **1997**, *9*, 3083–3095.

(25) Watzky, M. A.; Finke, R. G. Transition Metal Nanocluster Formation Kinetic and Mechanistic Studies. A New Mechanism When Hydrogen Is the Reductant: Slow, Continuous Nucleation and Fast Autocatalytic Surface Growth. *J. Am. Chem. Soc.* **1997**, *119*, 10382–10400.

(26) Finney, E. E.; Finke, R. G. The Four-Step, Double-Autocatalytic Mechanism for Transition-Metal Nanocluster Nucleation, Growth, and Then Agglomeration: Metal, Ligand, Concentration, Temperature, and Solvent Dependency Studies. *Chem. Mater.* **2008**, *20*, 1956–1970.

(27) Mozaffari, S.; Li, W.; Thompson, C.; Ivanov, S.; Seifert, S.; Lee, B.; Kovarik, L.; Karim, A. M. Colloidal Nanoparticle Size Control:

DOI: 10.1021/acs.jpcc.9b07683
J. Phys. Chem. C 2019, 123, 29954–29963

Experimental and Kinetic Modeling Investigation of the Ligand–Metal Binding Role in Controlling the Nucleation and Growth Kinetics. *Nanoscale* **2017**, *9*, 13772–13785.
(28) Lazzari, S.; Theiler, P. M.; Shen, Y.; Coley, C. W.; Stemmer, A.; Jensen, K. F. Ligand-Mediated Nanocrystal Growth. *Langmuir* **2018**, *34*, 3307–3315.
(29) Belloni, J.; Marignier, J.; Mostafavi, M. Mechanisms of Metal Nanoparticles Nucleation and Growth Studied by Radiolysis. *Radiat. Phys. Chem.* **2018**, DOI: 10.1016/j.radphyschem.2018.08.001.
(30) Alvarez, M. M.; Khoury, J. T.; Schaaff, T. G.; Shafigullin, M.; Vezmar, I.; Whetten, R. L. Critical Sizes in The Growth of Au Clusters. *Chem. Phys. Lett.* **1997**, *266*, 91–98.
(31) Alvarez, M. M.; Khoury, J. T.; Schaaff, T. G.; Shafigullin, M. N.; Vezmar, I.; Whetten, R. L. Optical Absorption Spectra of Nanocrystal Gold Molecules. *J. Phys. Chem. B* **1997**, *101*, 3706–3712.
(32) Yao, Q.; Yuan, X.; Fung, V.; Yu, Y.; Leong, D.; Jiang, D.; Xie, J. Understanding Seed-Mediated Growth of Gold Nanoclusters at Molecular Level. *Nat. Commun.* **2017**, *8*, 927.
(33) Van Hyning, D. L.; Klemperer, W. G.; Zukoski, C. F. Silver Nanoparticle Formation: Predictions and Verification of The Aggregative Growth Model. *Langmuir* **2001**, *17*, 3128–3135.
(34) Abkhalimov, E. V.; Parsaev, A. A.; Ershov, B. G. Preparation of Silver Nanoparticles in Aqueous Solutions in The Presence of Carbonate Ions As Stabilizers. *Colloid J.* **2011**, *73*, 1–5.
(35) Luo, Z.; Nachammai, V.; Zhang, B.; Yan, N.; Leong, D. T.; Jiang, D.-e.; Xie, J. Toward Understanding the Growth Mechanism: Tracing All Stable Intermediate Species from Reduction of Au(I)-Thiolate Complexes to Evolution of Au_{25} Nanoclusters. *J. Am. Chem. Soc.* **2014**, *136*, 10577–10580.
(36) Henglein, A.; Tausch-Treml, R. Optical Absorption and Catalytic Activity of Subcolloidal and Colloidal Silver in Aqueous Solution: A Pulse Radiolysis Study. *J. Colloid Interface Sci.* **1981**, *80*, 84–93.
(37) Mostafavi, M.; Dey, G. R.; François, L.; Belloni, J. Transient and Stable Silver Clusters Induced by Radiolysis in Methanol. *J. Phys. Chem. A* **2002**, *106*, 10184–10194.
(38) Stamplecoskie, K. G.; Scaiano, J. C. Kinetics of The Formation of Silver Dimers: Early Stages in The Formation of Silver Nanoparticles. *J. Am. Chem. Soc.* **2011**, *133*, 3913–3920.
(39) Laxson, W. W.; Finke, R. G. Nucleation is Second Order: An Apparent Kinetically Effective Nucleus of Two for $Ir(0)_n$ Nanoparticle Formation from $[(1,5\text{-COD})Ir^{I}\cdot P2W15Nb3O62]^{8-}$ Plus Hydrogen. *J. Am. Chem. Soc.* **2014**, *136*, 17601–17615.
(40) Besson, C.; Finney, E. E.; Finke, R. G. A Mechanism for Transition-Metal Nanoparticle Self-Assembly. *J. Am. Chem. Soc.* **2005**, *127*, 8179–8184.
(41) Yao, S.; Yuan, Y.; Xiao, C.; Li, W.; Kou, Y.; Dyson, P. J.; Yan, N.; Asakura, H.; Teramura, K.; Tanaka, T. *I*nsights into The Formation Mechanism of Rhodium Nanocubes. *J. Phys. Chem. C* **2012**, *116*, 15076–15086.
(42) Karim, A. M.; Al Hasan, N.; Ivanov, S.; Siefert, S.; Kelly, R. T.; Hallfors, N. G.; Benavidez, A.; Kovarik, L.; Jenkins, A.; Winans, R. E.; Datye, A. K. Synthesis Of 1 Nm Pd Nanoparticles In A Microfluidic Reactor: Insights From In Situ X-Ray Absorption Fine Structure Spectroscopy And Small-Angle X-Ray Scattering. *J. Phys. Chem. C* **2015**, *119*, 13257–13267.
(43) Wang, F.; Richards, V. N.; Shields, S. P.; Buhro, W. E. Kinetics and Mechanisms of Aggregative Nanocrystal Growth. *Chem. Mater.* **2013**, *26*, 5–21.
(44) LaGrow, A. P.; Ingham, B.; Toney, M. F.; Tilley, R. D. Effect of Surfactant Concentration and Aggregation on the Growth Kinetics of Nickel Nanoparticles. *J. Phys. Chem. C* **2013**, *117*, 16709–16718.
(45) Dass, A. Nano-Scaling Law: Geometric Foundation of Thiolated Gold Nanomolecules. *Nanoscale* **2012**, *4*, 2260.
(46) Morris-Cohen, A. J.; Vasilenko, V.; Amin, V. A.; Reuter, M. G.; Weiss, E. A. Model for Adsorption of Ligands to Colloidal Quantum Dots with Concentration-Dependent Surface Structure. *ACS Nano* **2012**, *6*, 557–565.
(47) Chen, J.; Zhang, Q.-F.; Bonaccorso, T. A.; Williard, P. G.; Wang, L.-S. Controlling Gold Nanoclusters by Diphospine Ligands. *J. Am. Chem. Soc.* **2014**, *136*, 92–95.
(48) Weare, W. W.; Reed, S. M.; Warner, M. G.; Hutchison, J. E. Improved Synthesis of Small (Dcore≈ 1.5 Nm) Phosphine-Stabilized Gold Nanoparticles. *J. Am. Chem. Soc.* **2000**, *122*, 12890–12891.
(49) Chevrier, D. M.; Raich, L.; Rovira, C.; Das, A.; Luo, Z.; Yao, Q.; Chatt, A.; Xie, J.; Jin, R.; Akola, J.; Zhang, P. Molecular-Scale Ligand Effects in Small Gold–Thiolate Nanoclusters. *J. Am. Chem. Soc.* **2018**, *140*, 15430–15436.
(50) Jin, R. Quantum Sized, Thiolate-Protected Gold Nanoclusters. *Nanoscale* **2010**, *2*, 343–362.
(51) Yin, Y.; Alivisatos, A. P. Colloidal Nanocrystal Synthesis and the Organic–Inorganic Interface. *Nature* **2005**, *437*, 664–670.
(52) Yu, Y.; Chen, X.; Yao, Q.; Yu, Y.; Yan, N.; Xie, J. Scalable and Precise Synthesis of Thiolated Au_{10-12}, Au_{15}, Au_{18}, and Au_{25} Nanoclusters via pH Controlled CO Reduction. *Chem. Mater.* **2013**, *25*, 946–952.
(53) Briñas, R. P.; Hu, M.; Qian, L.; Lymar, E. S.; Hainfeld, J. F. Gold Nanoparticle Size Controlled by Polymeric Au(I) Thiolate Precursor Size. *J. Am. Chem. Soc.* **2008**, *130*, 975–982.
(54) Tsunoyama, H.; Ichikuni, N.; Tsukuda, T. Microfluidic Synthesis and Catalytic Application of PVP-Stabilized, ∼1 Nm Gold Clusters. *Langmuir* **2008**, *24*, 11327–11330.
(55) Tofighi, G.; Gaur, A.; Doronkin, D. E.; Lichtenberg, H.; Wang, W.; Wang, D.; Rinke, G.; Ewinger, A.; Dittmeyer, R.; Grunwaldt, J.-D. Microfluidic Synthesis of Ultrasmall Au Nanoparticles with a Homogeneously Mixed Alloy Structure in Fast Continuous Flow for Catalytic Applications. *J. Phys. Chem. C* **2018**, *122*, 1721–1731.
(56) Pan, L.-J.; Tu, J.-W.; Ma, H.-T.; Yang, Y.-J.; Tian, Z.-Q.; Pang, D.-W.; Zhang, Z.-L. Controllable Synthesis of Nanocrystals in Droplet Reactors. *Lab Chip* **2018**, *18*, 41–56.
(57) Song, Y.; Hormes, J.; Kumar, C. S. S. R. Microfluidic Synthesis of Nanomaterials. *Small* **2008**, *4*, 698–711.
(58) Liu, Y.; Jiang, X. Why Microfluidics? Merits and Trends in Chemical Synthesis. *Lab Chip* **2017**, *17*, 3960–3978.
(59) Verwey, E. J. W. Theory of The Stability of Lyophobic Colloids. *J. Phys. Colloid Chem.* **1947**, *51*, 631–636.
(60) Pettibone, J. M.; Reardon, N. R. Nucleation Products of Ligated Nanoclusters Unaffected by Temperature and Reducing Agent. *Nanoscale* **2012**, *4*, 5593–5596.

DOI: 10.1021/acs.jpcc.9b07683
J. Phys. Chem. C 2019, 123, 29954–29963